

# WAVELET EXTRACTION BY SONIC LOG CORRELATION

DAN HAMPSON<sup>1</sup> AND MIKE GALBRAITH<sup>1</sup>

## ABSTRACT

Wavelets in seismic data can be estimated by a semideterministic approach in which various portions of a sonic log are correlated with corresponding portions of seismic data. A statistical measure, the effective length of the extracted wavelets, is used to estimate the reliability of the wavelets. This method of "stratigraphic deconvolution" was used to study the phase characteristics of seismic wavelets in two areas in the western Canada sedimentary basin.

In the first area, wavelets were extracted at four well locations on two seismic lines. The lateral reliability

of the method was investigated by comparing the average phases of the four extracted wavelets.

In the second area, a seismic line was processed through five different sequences and wavelets were extracted at a single well location to evaluate the consistency of the method when applied to the various processing sequences. Finally, the phase information of the extracted wavelets was used to compute zero-phase seismic sections.

---

## INTRODUCTION

In recent years, considerable interest has been generated in the problem of determining the phase characteristics of seismic wavelets accurately. Two factors largely account for this interest: first, the increasing need to extract detailed stratigraphic information from seismic data, and second, the realization that the phase assumptions implicit in statistical deconvolution schemes may not generally be valid, and that the resulting deconvolved sections may differ considerably from zero-phase. In this paper, a method of extracting a seismic wavelet by correlating seismic data with well-log data from a nearby well is discussed. This method does not make any phase assumptions about the wavelet, and thus attempts to gain objective information about the wavelet at the well location. After the wavelet extraction procedure has been described, the method is applied to two data cases: the first demonstrates the consistency of the wavelets extracted by using several wells in a given area; the second uses the method to decompose the seismic wavelet into its various components.

## WAVELET PHASE

The general objective of all wavelet processing or deconvolution programs can be summarized as shown in Figure 1. In the convolutional model, an input trace is considered to be the result of convolving an input wavelet with the earth reflectivity sequence and adding noise. Although both wavelet and noise are generally time-variant, it is common practice to consider them as fixed in some window on the trace. In wavelet processing the attempt is to recover not the reflectivity sequence itself, but rather an output trace which is simply an output wavelet convolved with the reflectivity sequence plus some new noise. Wavelet processing is successful to the extent that three criteria are satisfied:

- 1) the output wavelet should be zero-phase to ensure optimum resolution and ease of interpretation
- 2) the output wavelet should be broad-band (or equivalently, of short duration in time; *i.e.*, spiky)
- 3) the output signal-to-noise ratio should be high

<sup>1</sup>Veritas Seismic Processors Ltd.

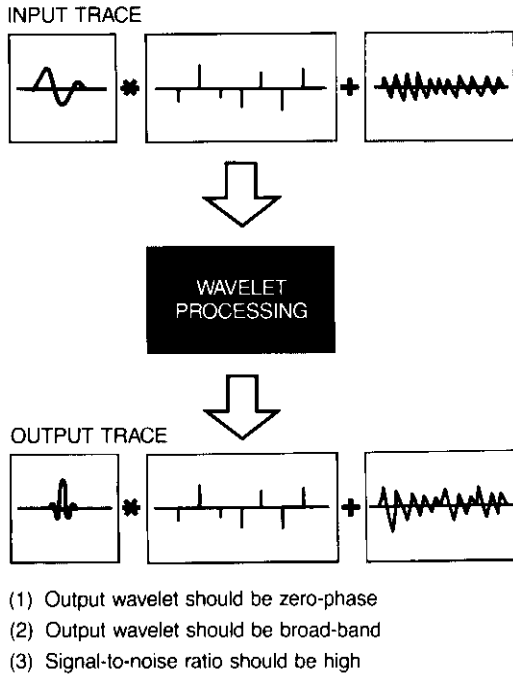


Fig. 1. Wavelet processing.

In most practical cases, the second and third criteria form a trade-off, and much work has been done on the problem of finding the optimum compromise between these two conflicting requirements. However, the first criterion is essentially independent of the others, and a deconvolution procedure that does very well at compressing the wavelet may produce a result that is far from zero-phase. Figures 2 and 3 show how a given amplitude spectrum may be combined with three different phase spectra to produce three different wavelets. The frequency domain representation is shown in Figure 2. Here, a single amplitude spectrum is shown (with its scale in dB on the right of Fig. 2), and the three phase spectra are "minimum-phase," -90 degree phase, and zero-phase. The corresponding time responses are shown in Figure 3. If these wavelets were deconvolution outputs, all three would satisfy the criterion of being broad-band, but only wavelet 3, the zero-phase wavelet, is the result desired in a wavelet processed section. Wavelet 3 can be called the "zero-phase equivalent" of the other two wavelets, and a deconvolved section that results in a wavelet of the type 1 or 2 may be phase-corrected to zero-phase, if the input phase can be deter-

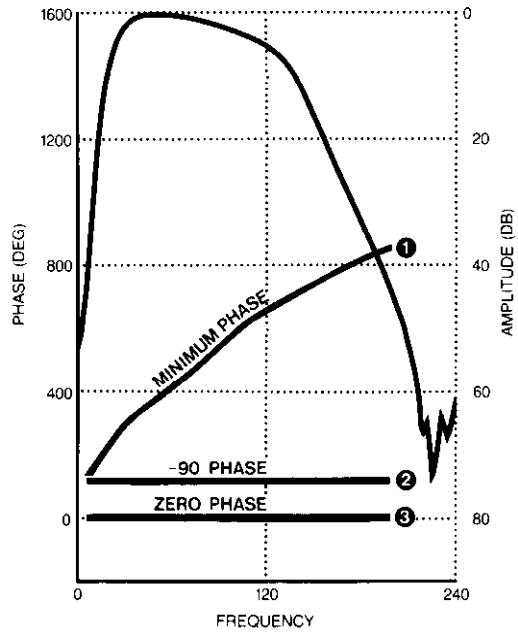


Fig. 2. Frequency domain (after Neale 1977).

mined accurately. This paper is essentially concerned with that problem of estimating the wavelet phase. To provide an idea of the significance of the final wavelet phase, Figure 4 shows synthetic traces generated from a sonic log by using a series of broad-band wavelets, all of which have the same amplitude spectrum, but different constant phase shift spectra. The wavelet phase is shown on the right of each panel. It is clear that three conclusions can be drawn from this figure:

- 1) as deconvolved outputs, all five synthetics are equally broad-band and noise free
- 2) the character and possible interpretation of various events change significantly as the phase is rotated through 180 degrees
- 3) in the absence of other independent information, it is difficult or impossible to determine the correct phase on the basis of the seismic traces alone

The technique described below attempts to estimate the correct phase by utilizing geological information in the form of well-log data.

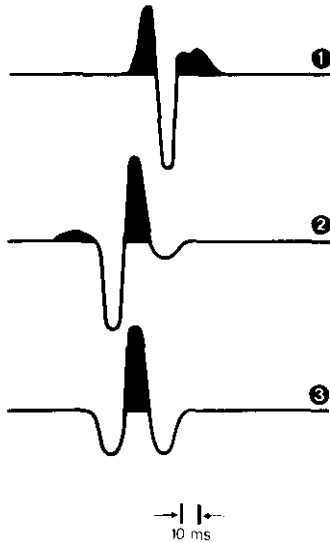


Fig. 3. Time domain.

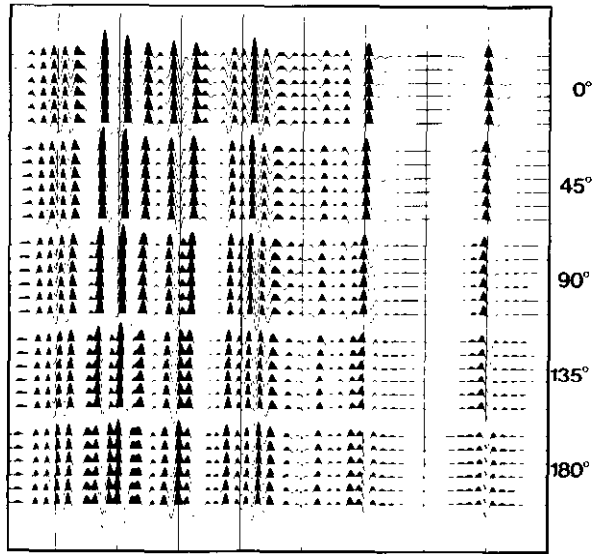


Fig. 4. Constant phase synthetics.

WAVELET EXTRACTION TECHNIQUE

In the convolutional model, the seismic trace can be written in the form

$$T = W * R + N \quad (1)$$

where  $T$  = seismic trace  
 $W$  = wavelet  
 $R$  = reflection coefficient sequence  
 $N$  = noise

The difficulty in estimating  $W$ , or  $R$ , stems from the fact that there are three unknowns in this single equation. The noise,  $N$ , can never be estimated precisely, but must be described statistically. The reflectivity sequence, on the other hand, can be estimated by using the impedance function calculated from a sonic and density log, in the same manner as when calculating a synthetic seismogram. If the reflectivity sequence calculated from the log is close to the "true" reflectivity sequence in the seismic data, and if the noise in the seismic data is low-amplitude, random, and uncorrelated with the other components, then the true wavelet,  $W$ , is the one that makes the synthetic seismogram match the seismic trace as closely as possible. Figure 5 illustrates this concept.

A synthetic is formed from a well log and matched with seismic data that tie the well. In

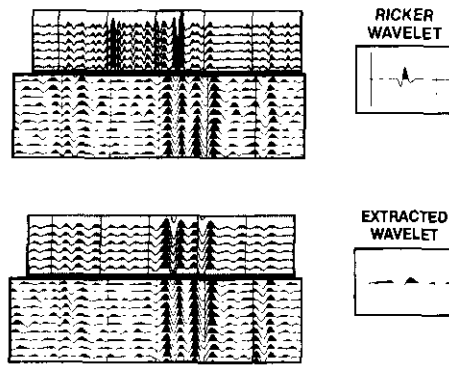


Fig. 5. Synthetics correlated with seismic data.

the upper case, a broad-band Ricker wavelet is used, and we see that, although the events line up generally in the right places, the character does not match properly. The lower case shows the same seismogram formed with a different wavelet. Since the character match is much better, we say that the lower wavelet in Figure 5 is a much better estimate of the seismic wavelet than the Ricker wavelet above. Having estimated the wavelet in this way, we can then calculate the phase correction necessary to transform it into the zero-phase equivalent wavelet,

as shown in Figure 6. Here the same phase correction is applied to both the synthetic and the seismic data. The effect of this correction is to change the extracted wavelet into a zero-phase wavelet with the same amplitude spectrum, as shown on the right of the figure. The tie between the phase-corrected seismic data and the phase-corrected synthetic remains as good as in Figure 5 but, now, since the wavelet in the synthetic is zero-phase, we conclude that the seismic data are zero-phase as well.

Mathematically, the wavelet extraction problem is formulated as shown in Figure 7. The general least-squares shaping problem is: given an input sequence A, and a desired output sequence B, design a filter F which transforms A into B:

$$A * F \simeq B$$

such that the error sequence

$$E = B - A * F$$

has minimum energy; *i.e.*,

$$\sum_i E^2(i) = \text{minimum.}$$

In the ideal case shown in Figure 7, the input sequence is the well-log reflectivity sequence, the desired output is the seismic trace, and the result is the extracted wavelet.

In practice a number of problems arise that can seriously degrade the results. These can be: errors in the well-log reflectivity sequence that invalidate the assumption that it is a good estimate of the earth reflectivity sequence, random noise, and long-period multiples, etc. in the seismic data, which may be considered as increasing the noise term in equation (1) above. Experience has shown that problems in the log, particularly errors in the depth-to-time conversion, cause the most difficulty. This type of problem arises because the log is measured as a function of depth, and accurate velocity information is needed to calculate the reflectivity sequence as a function of two-way time. Normally, the transit-times themselves supply this velocity information. Thus, errors in the transit-times from phenomena such as caving, secondary porosity, and so forth can distort the time-scale, resulting in the familiar "stretch" in the derived synthetic. Of course, additional information from a check-shot survey can be used to calibrate the log, but this provides only a gross correction, and an algorithm must be devised that will converge to a good wavelet estimate in

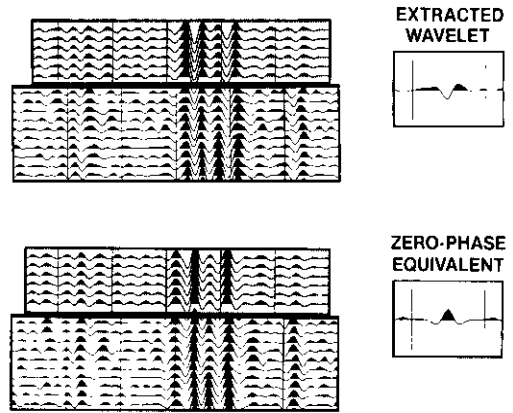


Fig. 6. Correcting to zero-phase.

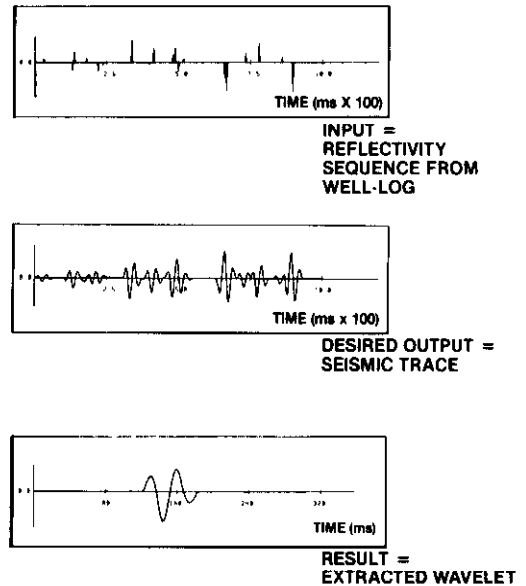


Fig. 7. Wavelet extraction by least-squares shaping filter.

spite of the small but nonetheless significant discrepancies between the log and the seismic data.

Figure 8 illustrates one approach. The reflectivity sequence is the same as that in Figure 7, except that a 20 ms time delay has been inserted in the region between 500 ms and 700 ms as

shown. This type of error is consistent with the observation that often the distorting influences in the log occur in the form of specific regions of erroneous measurements due to local bore-hole or lithologic conditions. The seismic trace has been repeated as in Figure 7, except that a small amount of random noise has been added. In calculating the shaping filter, the choice exists to use all or part of the log as the design window, and Figure 8 shows the resultant wavelets when various windows are used. Generally, when a window is large enough to encompass parts of the log that are time-shifted with respect to each other, a distortion results in the wavelet, as shown in the first case. On the other hand, when the window becomes very short, as in the fourth case, the statistical errors in the auto- and cross-correlation estimates introduce a large background noise level. Windows such as cases 2 and 3, which are as long as possible without overlapping the time shift, give the best estimates of the wavelet. It can be seen that wavelet 3 is shifted 20 ms with respect to wavelet 2, and this simply results from the fact that the log window for this wavelet is in "error" by 20 ms. In general, the quality of the extracted wavelet depends on the length and location of the design window.

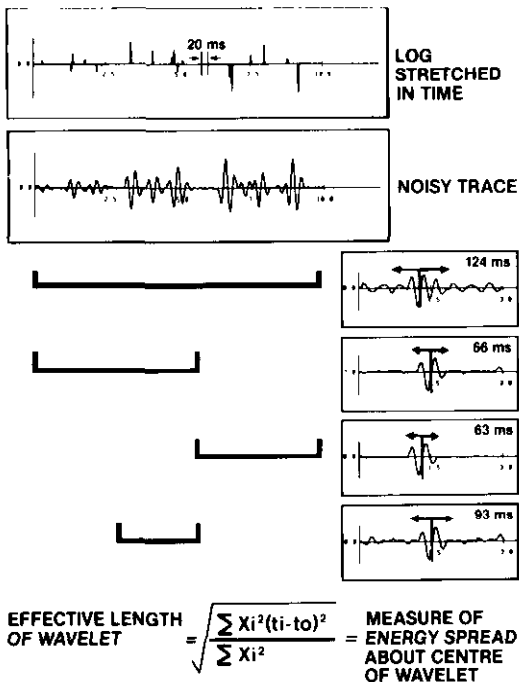


Fig. 8. Effect of errors on wavelet extraction.

It can be seen, particularly in wavelets 2, 3 and 4, that while the basic wavelet shape remains the same, it is the background energy or "noise" that varies from window to window. This observation leads to a criterion for evaluating wavelets from different windows: a good wavelet estimate is one that has a minimum of background noise or, equivalently, a larger proportion of its energy concentrated in the centre. This criterion is quite reasonable from another point of view: the extracted wavelet varies directly with the cross-correlation between log and seismic trace, and a concentration of energy in the centre of the cross-correlation indicates that the log and trace are in fact related by a short convolutional operator.

A mathematical measure of the spread of energy in the wavelet is the "EFFECTIVE LENGTH" defined by Berkhout (1977):

$$L^2 = \frac{\sum X_i^2 (t_i - t_0)^2}{\sum X_i^2}$$

- Where
- $t_i$  = time corresponding to  $i$ -th sample
  - $t_0$  = time corresponding to time zero on the wavelet
  - $X_i$  = sample value at the  $i$ -th position

and the sums are over-all samples in the extracted wavelet. The computed value  $L$  is in units of time, and measures the root-mean-square "distance" of the samples from time zero. For a two-sided wavelet, multiplying  $L$  by two gives the effective spread of the wavelet energy. The magnitude of  $L$  depends on the choice of  $t_0$ , although for the purposes of comparing several extracted wavelets the actual choice of  $t_0$ , is not critical as long as it is chosen consistently on the various wavelets. In this paper the time zero on a wavelet is chosen in such a way as to remove the wavelet's average linear phase. This point is further discussed in the appendix.

The effective length calculated for each of the extracted wavelets is indicated in Figure 8. We can see that, in fact, the effective length does decrease as the wavelet approaches the "true wavelet", as shown in Figure 7.

The use of this approach on a real data case is indicated in Figure 9. What is shown is a series of 36 wavelets extracted from various windows by using a single impedance log and a single seismic trace. The relevant portion of the calcu-

lated reflectivity sequence that was used extended from 800 ms to 1800 ms. Within this 1000 ms section, 36 windows were tried out, varying in length from 300 ms to 1000 ms. In each case a wavelet was extracted; and they are shown on the left of the figure. The bar diagram on the right indicates the particular window used; for example, the first wavelet used a window from 800 to 1100 ms, the second a window from 900 to 1200 ms, and so on. The last 300 ms window extended from 1500 ms to 1800 ms, and then a series of 400 ms windows follows. It can be seen, especially on the window lengths greater than 400 ms, that the basic wavelet shape remains consistent in the centre, while the background noise varies. Four of the wavelets are repeated at the bottom of the figure, and their calculated effective lengths indicated. Of the four, the optimum window extended from 1000 to 1500 ms, with the shorter and larger windows showing slightly higher background noise. The wavelet from 800 to 1100 ms is particularly long, indicating a poor correlation due to errors in the shallow part of the log.

In practice, this procedure can be repeated by using several traces from the vicinity of the log. Figure 10 shows the result of taking all the wavelets extracted in Figure 9, as well as those from 11 other traces in the vicinity of the well, and reordering them on the basis of the calculated effective length, from shortest onward. Only the first 40 and the last 40 wavelets are shown. The shortest effective length is 64 ms

and the longest 156 ms. The window diagram indicates that, on average, the better wavelets come from the region from 1000 ms to 1500 ms, as in the previous figure. The basic wavelet shape tends to remain consistent as the background noise level rises, and can be discerned even in the poorest wavelets at the bottom of the figure.

Finally, the first 100 wavelets of this reordered set have been averaged to form the wavelet shown at the bottom of the figure. This averaging procedure tends to result in a wavelet with a yet shorter effective length, as the background noise is uncorrelated. This wavelet then is taken as the final extracted wavelet, and can be considered as an average wavelet derived from a two-dimensional window, extending from 1000 ms to 1500 ms in time, and from a region in space extending 6 traces on either side of the well location.

The wavelet extraction procedure is summarized as follows:

- 1) Extract wavelets by using a large number of windows with varying lengths and locations.
- 2) Reorder the wavelets from shortest effective length onward.
- 3) Average those wavelets whose effective lengths are shorter than some specified value.

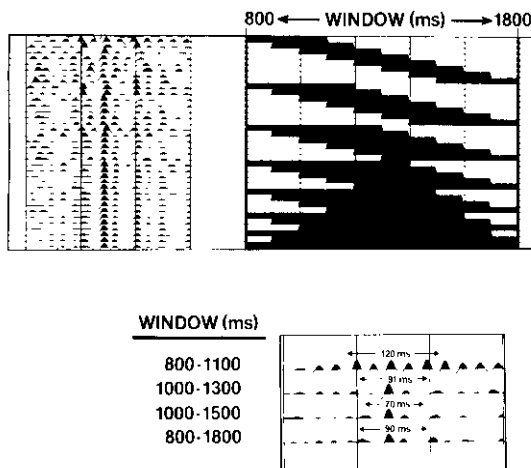


Fig. 9. Wavelets extracted from 36 windows.

APPLICATIONS

Case 1

To demonstrate the wavelet extraction method on real data, two cases are described. The first involves two lines of seismic data and four wells, as shown in Figure 11. The wells were located roughly on the corners of a rectangle with dimensions 4 mi by 1 mi. The two lines were processed identically by using spiking deconvolution before stack. Figure 12 shows the east end of line 1, with a synthetic formed from the sonic log at well 1 by using a zero-phase bandpass wavelet. The four well-logs were edited to eliminate the over-all stretch problems, and the tie shown in Figure 12 is typical of the four. It can be seen that the timing of the events is right, but there is a general character mismatch, due presumably to having used the wrong wavelet in the synthetic.

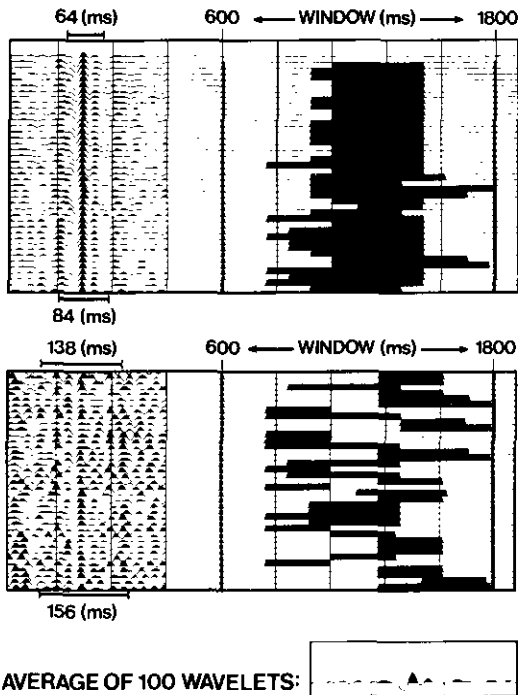


Fig. 10. Wavelets reordered by using effective length criterion.

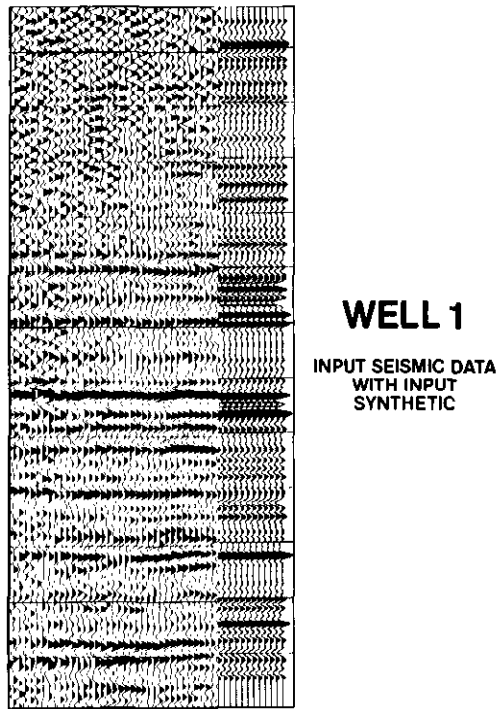


Fig. 12. East end of line 1 in Figure 11, showing input seismic data with input synthetic.

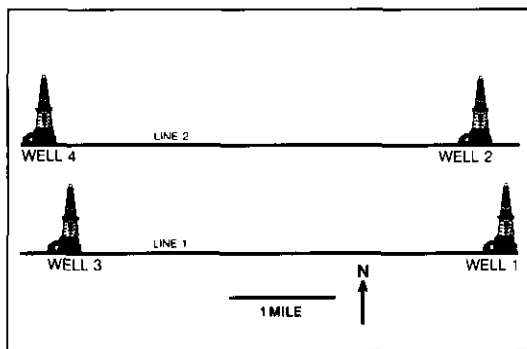


Fig. 11. Wavelet-extraction method applied to real data from four wells.

Some of the extracted wavelets from the four wells are shown in Figures 13 and 14. These wavelets have been extracted from a number of windows around each well location, and reordered by using the effective length criterion described earlier. Thus Figures 13 and 14 show the "best"

wavelets for each location. In each case, the first wavelet shown is the average wavelet calculated by adding the 100 best wavelets that follow, the second wavelet is a "model" wavelet used to align the extracted wavelets before averaging, and the extracted wavelets are plotted from trace 3 onward.

The window diagrams show that, although the maximum allowed window ranged from 600 to 1800 ms, the good wavelets came from a region from about 900 to 1500 ms. Within this region, differences occur because of the differences in fit between the various logs and the seismic data. For example, wells 1 and 3 used the deeper data down to 1500 ms, while wells 1 and 4 tended to use shorter windows than well 3. The extracted wavelets from the four wells show generally good consistency within a group, and from well to well.

Figure 15 shows the four extracted wavelets along with the over-all average wavelet formed by summing the four. It is clear that the wavelet shape is remarkably consistent, and that

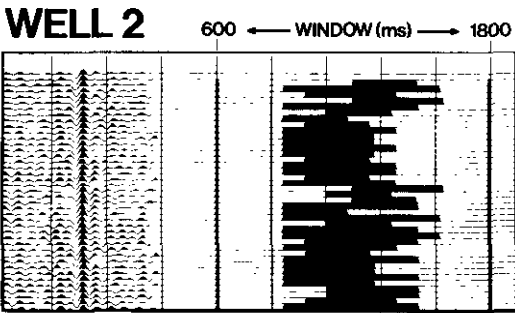
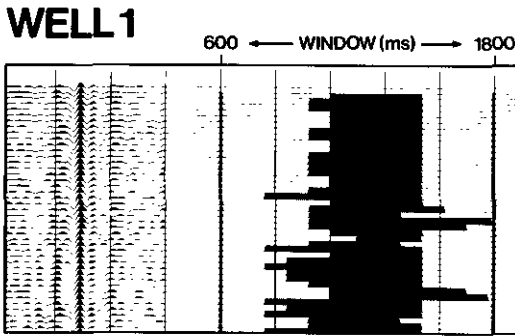


Fig. 13. Extracted wavelets from wells 1 and 2 in Figure 11.

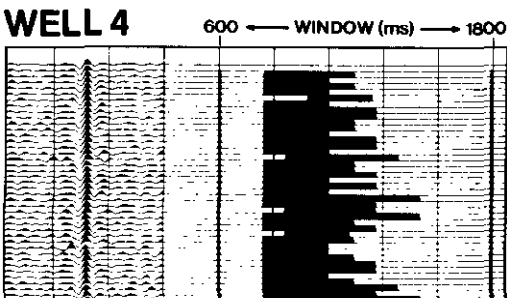
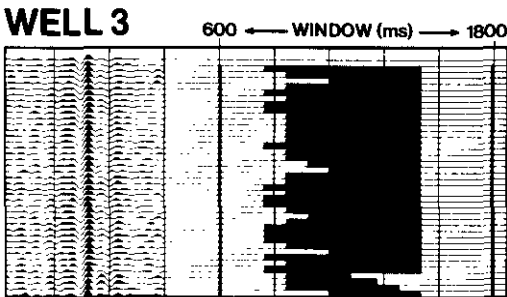


Fig. 14. Extracted wavelets from wells 3 and 4 in Figure 11.

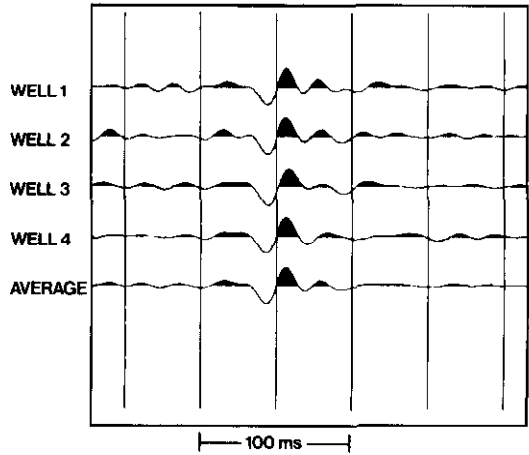


Fig. 15. Wavelets extracted from four wells in Figure 11, with their over-all average.

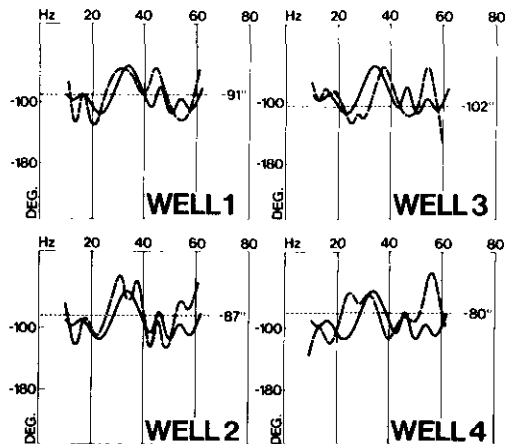


Fig. 16. Phase spectra of wavelets in Figure 15.

the differences between the wavelets occur mainly in the lobes following the major energy. It is possible that these differences arise from interbed multiple energy, which varies from place to place on the seismic data. In any event, the over-all average wavelet shows a good attenuation of those lobes that are not consistent in the four wavelets.

Figure 16 shows a plot of the phase spectra calculated by using the four wavelets. The zero time was taken as that which removes the average linear component (as described in the appendix) and corresponds roughly to the zero-crossing in the centre of the wavelets in Figure 15. The phase spectrum of the average wavelet was also

calculated, and is plotted as a solid line on each of the four graphs, while the individual spectra are plotted as a broken line. In each case, a line was fitted through the measured phase values in such a way as to minimize the total squared error, by using the amplitude spectrum as a weighting function. Consequently, only phase information from approximately 20 to 50 Hz was used for the line-fitting. Although there are obviously significant variations in the calculated phase spectra, it is also clear that the general trend in the four spectra is consistent, a fact shown by the spectrum of the average wave-

let. In particular, the linear approximation varies from  $-80$  to  $-102$  degrees, showing only a 22-degree total range, while the linear fit through the average wavelet spectrum measures  $-88$  degrees. At present, it is not clear to what extent the wiggles in the calculated spectra represent real variations in the local wavelet as opposed to local errors in the tie between well-log and seismic data.

Finally, Figure 17 shows the effect of using the average extracted wavelet to dephase the seismic data around Well 1. The upper part of

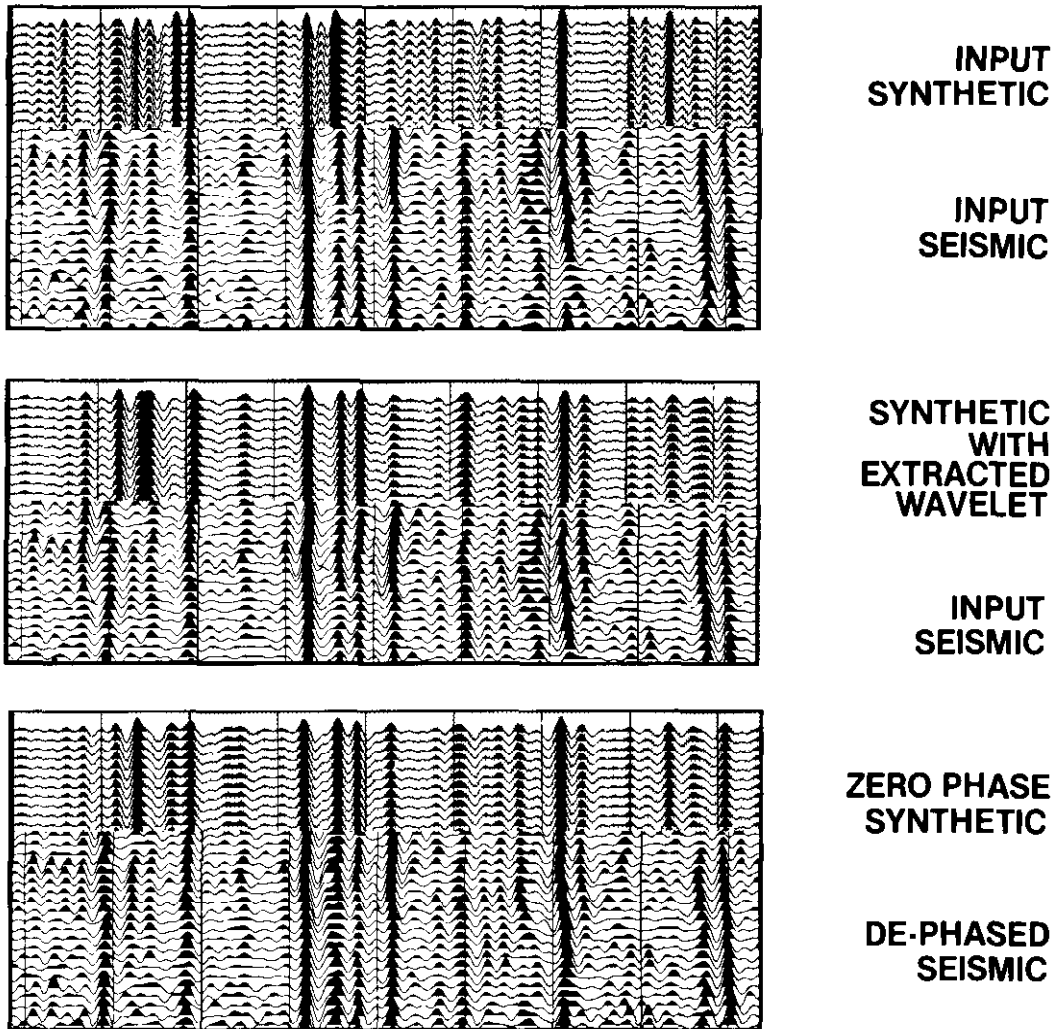


Fig. 17. Effect of using the average extracted wavelet to dephase the seismic data around well 1.

the figure shows the input seismic and input synthetic repeated from Figure 12. The second part of Figure 17 shows the same seismic data, but now a new synthetic has been formed by using the average extracted wavelet. The character tie is clearly improved over the entire section displayed.

In the lower panel, both seismic data and synthetic have been dephased by using the phase spectrum calculated from the average wavelet. The major difference appears to occur at the reflection approximately 200 ms from the bottom of the displayed section, where the reflection amplitude has increased significantly. This change in the seismic data is entirely consistent with the corresponding change in the synthetic, and indicates the type of improved resolution that can result from the dephasing process.

*Case 2*

One major benefit offered by this wavelet extraction method is the possibility of objectively evaluating the performance of various processing sequences. In particular, a wavelet extracted from a given processed section may be judged

according to the criterion specified earlier for the ideal output wavelet. This procedure is demonstrated in the following real data example, where a single well-log and seismic data set are used to estimate the phase contributions from various components of the seismic wavelet.

The seismic wavelet is considered to be the result of a series of processes, as indicated in Figure 18. Each component contributes its own impulse response or "wavelet", and the final result is the convolution of the individual wavelets. In the frequency domain, the phase spectrum of the final wavelet is the sum of the individual phase spectra. Figure 18 shows four basic categories into which the various factors affecting the wavelet could be grouped. They are

- 1) the source and near-surface, comprising the source signature, near-surface attenuation, ghost-resonance, etc.
- 2) the earth filter, comprising all other earth effects on the wavelet attenuation, multiples, etc.
- 3) the recording system response

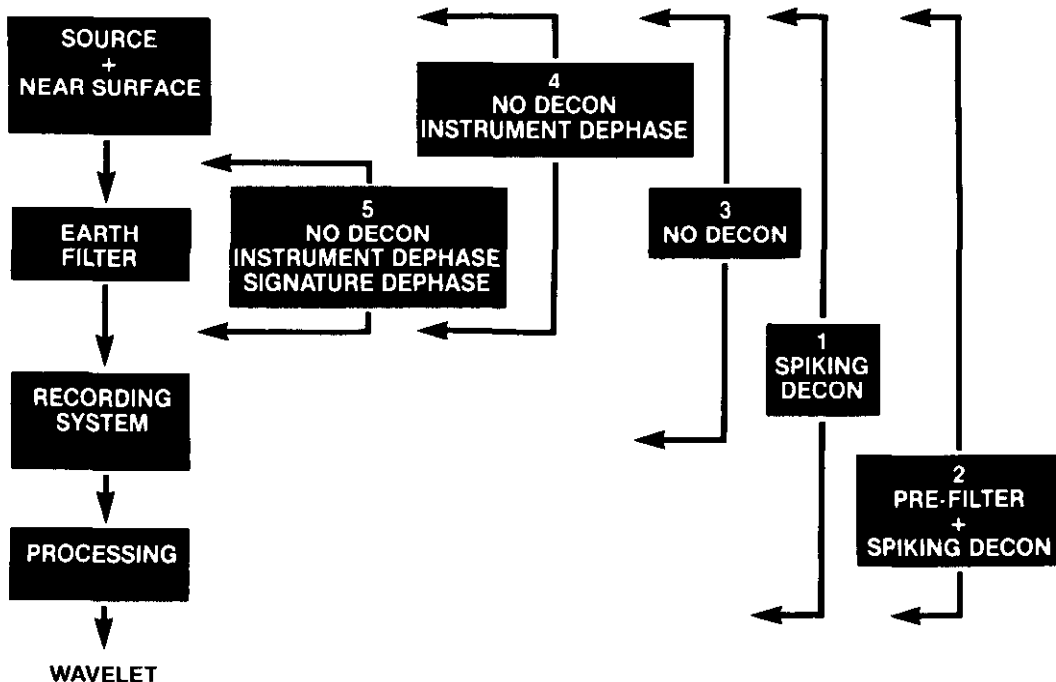


Fig. 18. Wavelet phase components.

## 4) the processing (especially deconvolution)

In order to study the relative phase contribution of each component, a seismic section was processed through the various sequences shown in Figure 18. The standard processing operation that affects the phase of the seismic wavelet is deconvolution, and two cases are used here: one in which the data are pre-filtered before spiking deconvolution (Section 2), and one with spiking deconvolution but no pre-filter (Section 1). The wavelets from these two sections include all four components. The third section (Section 3) was processed without deconvolution, so that the phase of its wavelet is affected only by the first three components. Section 4 was processed without deconvolution but with instrument dephasing, so that its wavelet contains the phase contributions of the source, near-surface, and earth filter. Finally, an estimate was made of the source and near-surface wavelet by direct measurement, and the compensation of this phase component produced section 5 which, in theory, contains the contribution of the earth filter alone.

The objective in measuring the source wavelet was to estimate the average phase contribution to the seismic wavelet from this component alone. For this purpose, wavelets were measured at a series of shot locations during the conventional shooting, by a single geophone suitably damped to ensure that the system was not overdriven. The phone was offset 110 ft from the source, which was a 10-lb charge. Figure 19 shows some of the measured wavelets on the left, time-shifted 120 ms for convenience. It is clear that the wavelet character is fairly consistent. On the right of Figure 19, the same wavelets are shown after removing the phase effect of the recording system. They have also been re-aligned by a cross-correlation method in order to calculate the average wavelet. Figure 20 shows the resulting wavelet, whose phase represents the average contribution of the source and near-surface. Because of the averaging procedure, the total time delay is not meaningful, but the phase-spectrum plot in Figure 20 indicates that the phase is very close to linear over the seismic band, which for the purposes of this study is taken as 15 to 45 Hz. As indicated, the measured source wavelet can be closely approximated by a 109-degree phase rotation.

A similar analysis has been performed on the recording system impulse response. Figure 21 shows the recording system and geophone pa-

rameters. Once again, the phase spectrum has been plotted and a straight line fitted through the portions of the curve from 15 to 45 Hz. This line intersects the phase axis at 112 degrees, indicating that the effect of the recording system on the seismic data in this bandpass is approximately a 112-degree rotation.

Finally, Figure 22 shows a similar analysis performed on the average spiking deconvolution operator applied to the seismic data to produce section 2 (prefilter + spiking decon). The prefilter used was an 8/12-60/65 bandpass filter and the decon operator was 80 ms long with 1% prewhitening. Since the deconvolution was done before stack, the actual operator varied from trace to trace, and the operator shown in Figure 22 is the average from several shots in the vicinity of the well. The phase spectrum is far from linear, but a straight line can be consistently fitted through the portion from 15 to 45 Hz, indicating that the average phase effect within this bandpass was  $-95$  degrees.

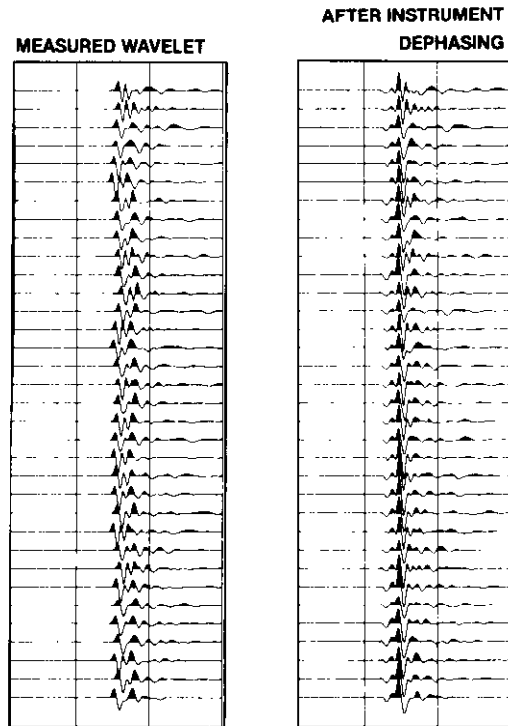


Fig. 19. Near-field wavelets measured by single geophone on surface.

Figure 23 shows the "conventionally processed" seismic data — this is the section processed with spiking deconvolution but no prefilter. Also shown is the wavelet that was extracted by using a sonic log from a well that is on the line. The synthetic created from that well by using the extracted wavelet is shown inserted at the well location. It can be seen that the match is very good, especially in the lower part of the well. It is also obvious that the wavelet is not zero-phase.

Figure 24 shows the result of dephasing the seismic data and synthetic, using the extracted wavelet phase. The resultant zero-phase wavelet is also shown. It is clear that the character has changed considerably over the entire section. It also appears that in some areas the reflection quality has improved. In particular, the event that intersects the deepest part of the log shows considerable improvement in continuity. A possible interpretation here is that this represents a single positive reflection coef-

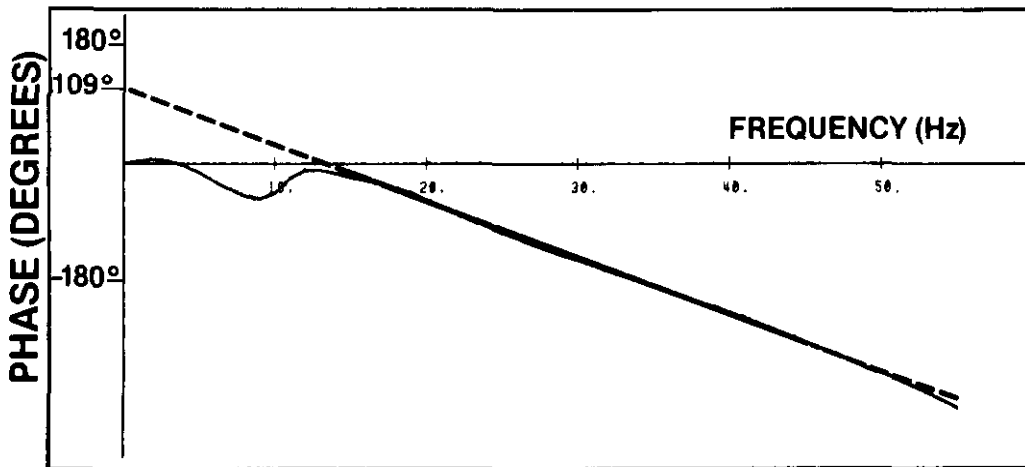
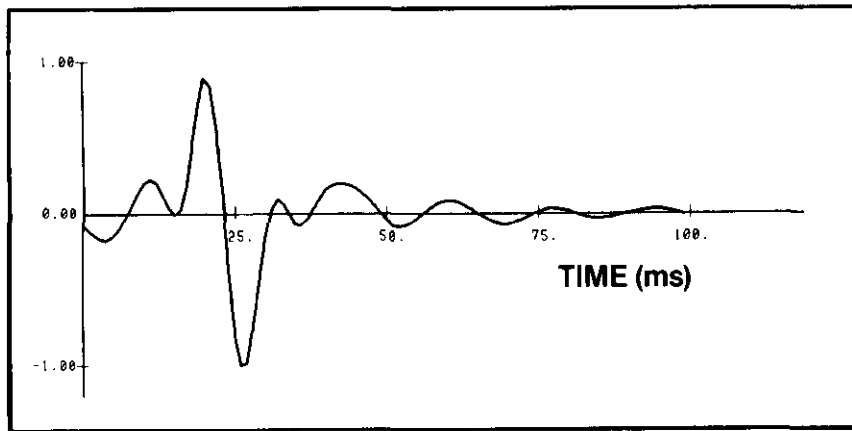


Fig. 20. Measured source signature (top) and phase spectrum (bottom) after instrument dephasing.

ficient, and the zero-phase wavelet gives the optimum resolution of that event. In general, the zero-phase section represents a good approximation of the filtered reflectivity sequence, as evidenced by the match with the zero-phase synthetic.

To see the result of the various processing procedures outlined earlier, a portion of the seismic data from the vicinity of the well was chosen. Figure 25 shows the resulting sections along with the extracted wavelet in each case.

The two spiking decon cases differed in that Case 1 used a 40-ms operator length and no prefilter, while Case 2 used an 80-ms operator length with the prefilter mentioned earlier. Tests indicated that it was the use of the prefilter, and not the operator length, that was crucial in bringing about the large phase difference between the two. This is entirely consistent with the fact that the minimum phase operator is derived from the amplitude spectrum of the data.

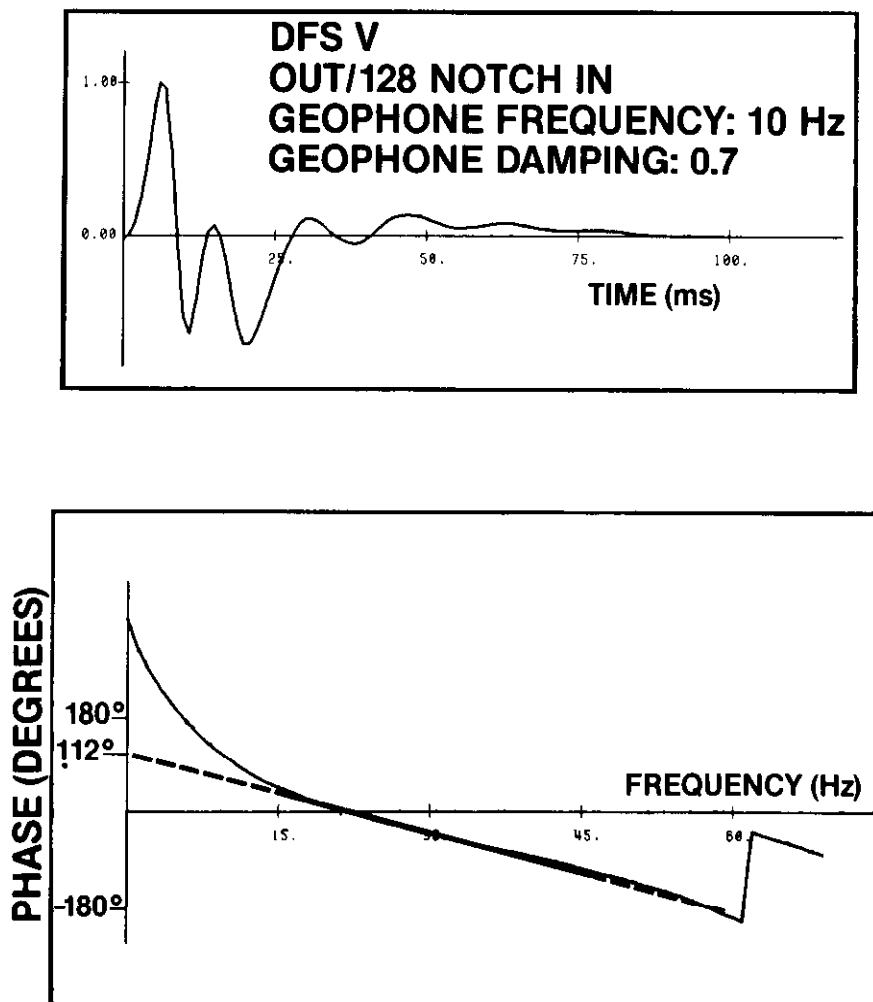


Fig. 21. Recording system response (top) and phase spectrum (bottom) after instrument dephasing.

It is clear from these sections that the various processing sequences produce a continuous change of wavelet character. It is also clear that all the results are far from zero-phase, except the fifth one, which used a deterministic measure of the instruments and source signature phase to make the phase correction. In particular, it appears that the final phase of the spiking deconv section depends critically on the use of prefilters, although it is not clear that any particular choice of parameters would produce a zero-phase result.

To verify that, in fact, the extracted wavelets represent good estimates of the wavelet phase, each section was dephased by using its own extracted wavelet. The result is shown in Figure 26. It is clear that the characters of all five sections are extremely similar. Sections 1 and 2 have been deconvolved, and this is evident in the higher frequency content. However, it is interesting to observe the similarity between these two sections, indicating that the two processing sequences affected mainly the wavelet phase, and that this difference could be

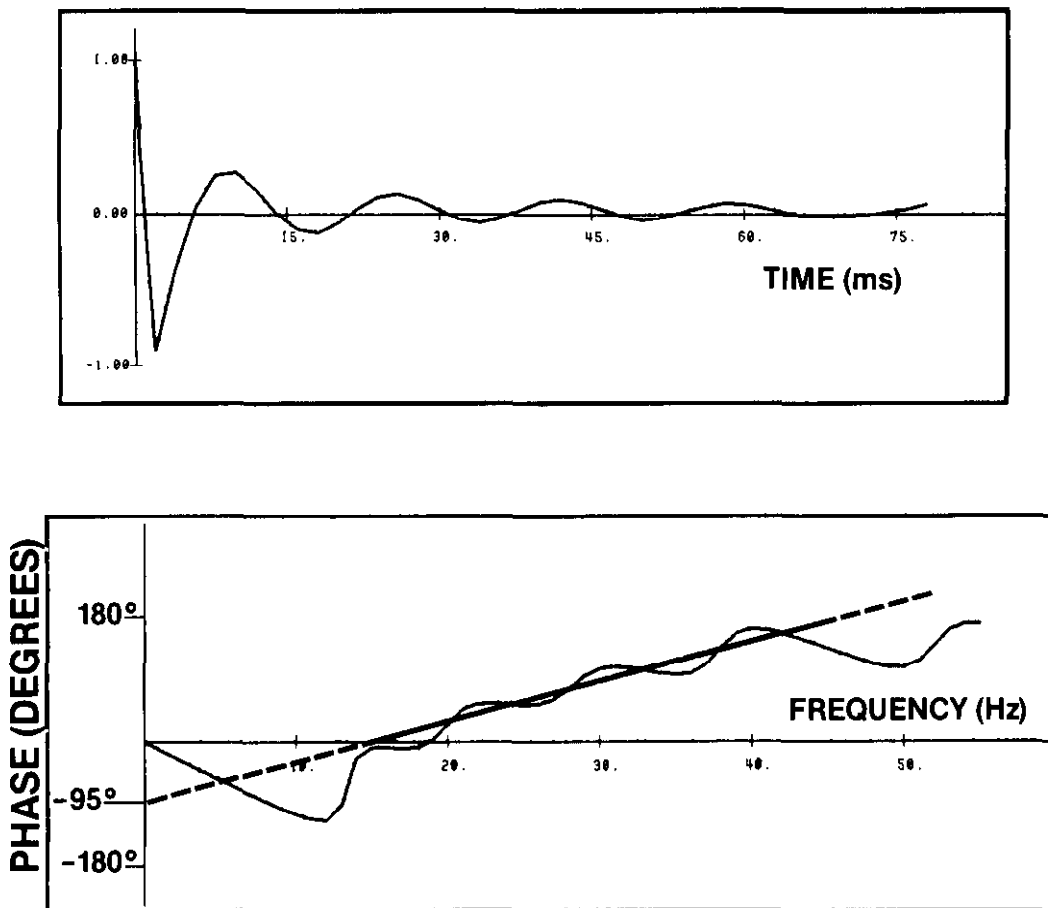


Fig. 22. Spiking deconvolution operator (top) and phase spectrum (bottom) after instrument dephasing.

corrected by using the wavelet-extraction technique.

The extracted wavelet information is summarized in Figures 27 and 28. The wavelet for each processing sequence is shown, along with the average linear phase calculated by using the phase spectrum from 15 to 45 Hz, as before.

The calculated phase values for the known wavelet components are also shown. The table in Figure 28 verifies the consistency of the extracted phase information. For example, the phase difference between wavelet 4 and wavelet 5 is 109 degrees, which happens to be exactly equal to the calculated source and near-surface wavelet phase. Similarly, the measured

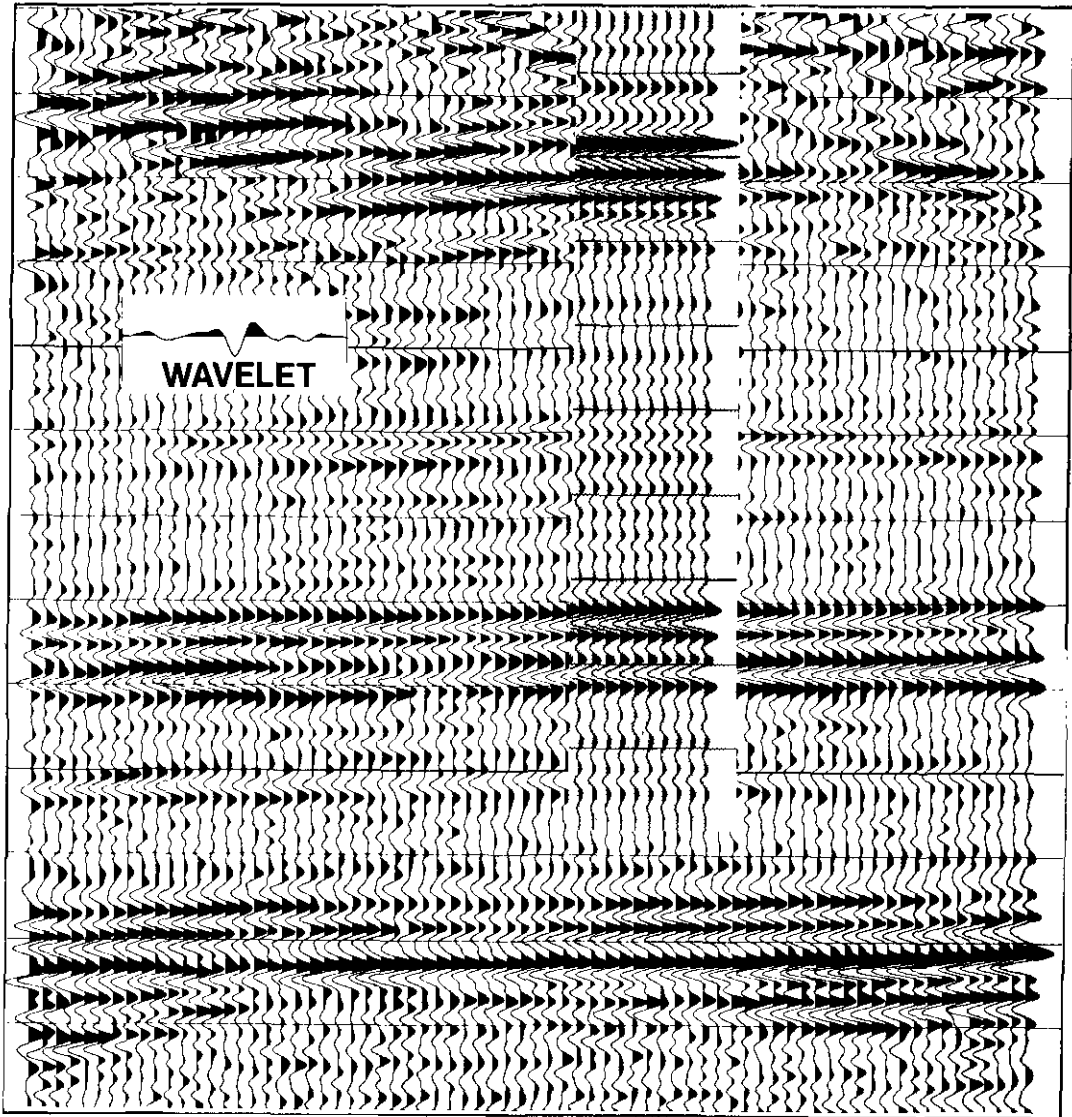


Fig. 23. Input seismic data with synthetic.

phase difference between wavelet 3 and wavelet 4 is 119 degrees, while the known phase shift for the recording system is 112 degrees, indicating an error of 7 degrees in this measurement. Finally, the measured difference between wavelet 3 and wavelet 2 is -87 degrees, compared with the calculated -95-degree phase shift for the deconvolution operator. These re-

sults verify that the phase differences introduced into the various sections have been accurately estimated by the extracted wavelets. In view of the statistical nature of the linear fit to the phase spectrum, these results are extremely encouraging and indicate that the extracted wavelet information can be used with some confidence.

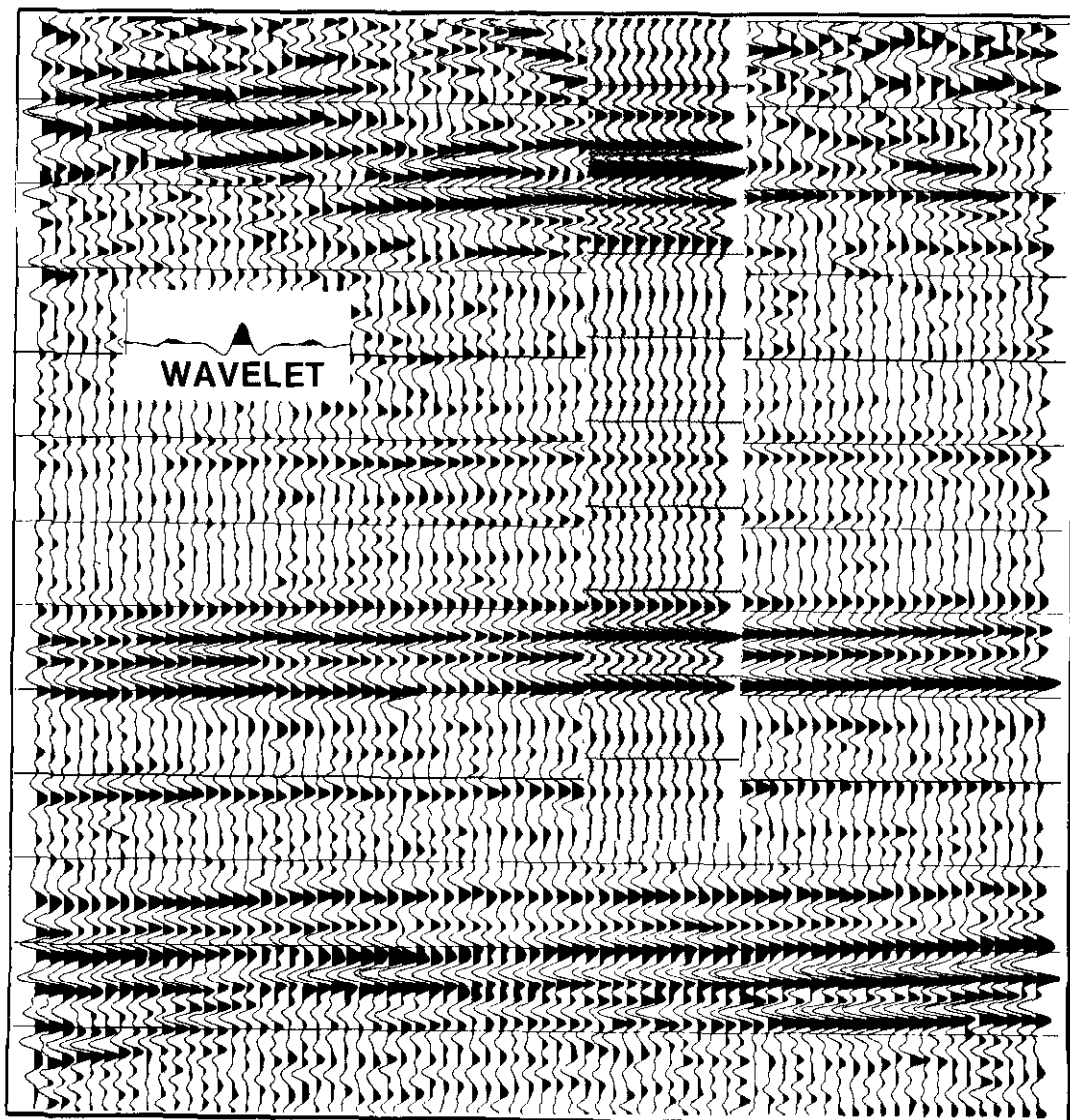


Fig. 24. Dephased seismic data with dephased synthetic.

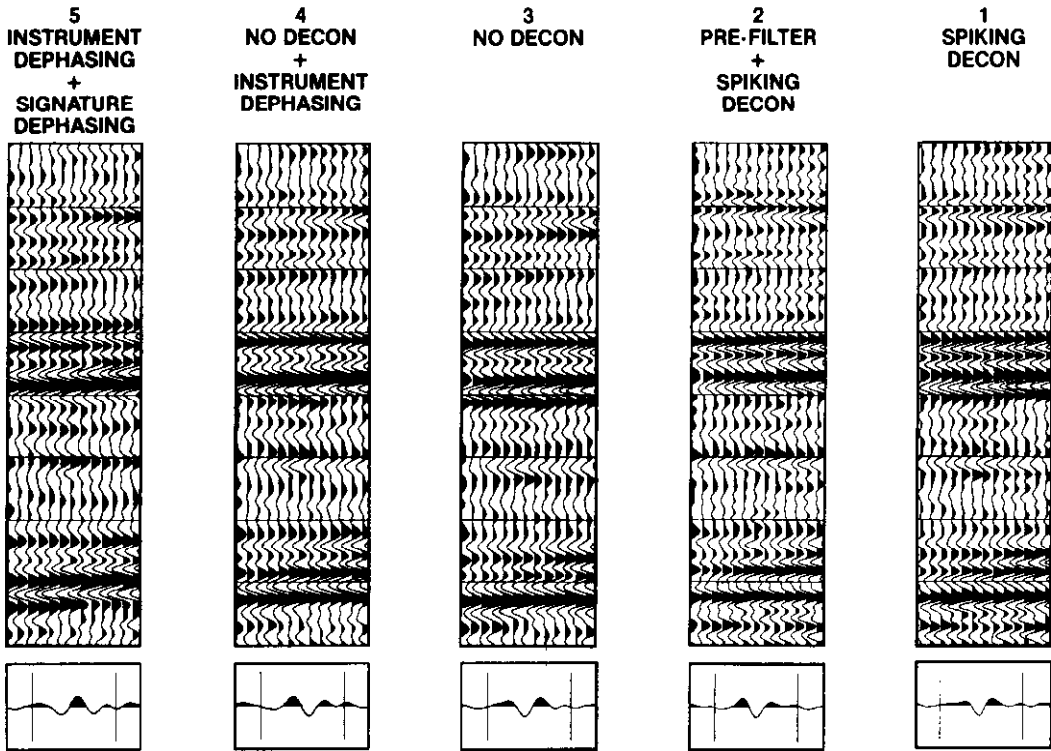


Fig. 25. Results of applying the various processing procedures to some of the seismic data from the vicinity of well 1.

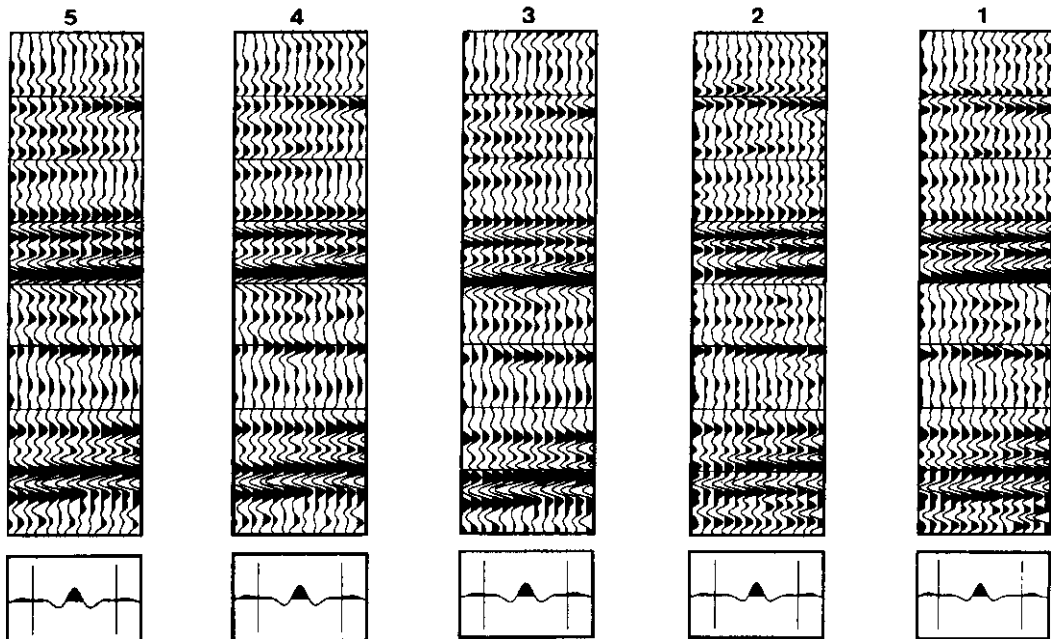


Fig. 26. Results of dephasing the five sections in Figure 25 by using their respective extracted wavelets.

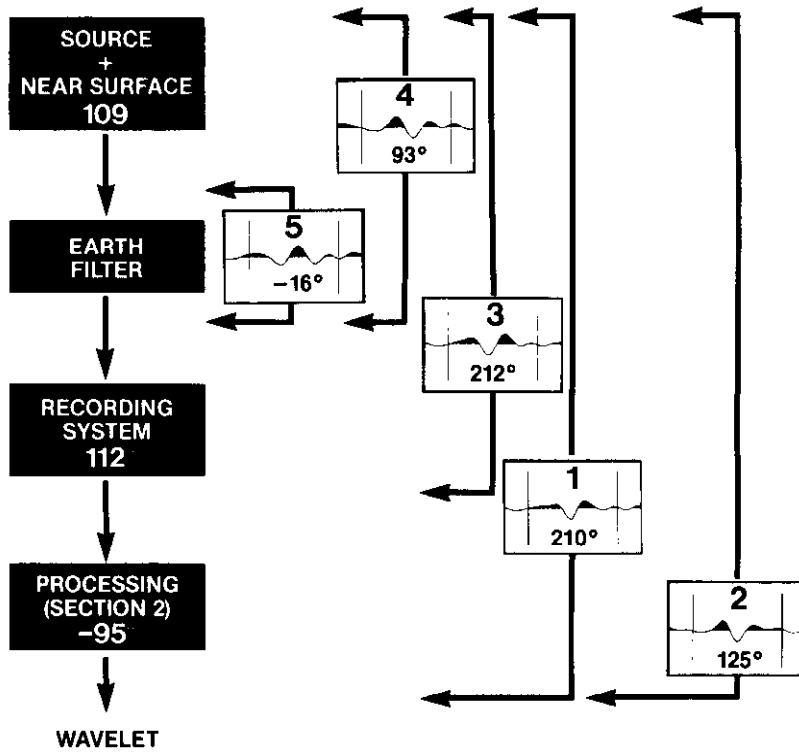


Fig. 27. Information obtained by wavelet-extraction technique.

		PHASE DIFFERENCES USING KNOWN WAVELETS	ERROR
<div style="border: 1px solid black; padding: 5px; display: inline-block;">                     4 NO DECON INSTRUMENT DEPHASE 93°                 </div> - <div style="border: 1px solid black; padding: 5px; display: inline-block;">                     5 NO DECON INSTRUMENT DEPH SIG. DEPH -16°                 </div> = 109°	SOURCE + NEAR SURFACE 109°	0°	
<div style="border: 1px solid black; padding: 5px; display: inline-block;">                     3 NO DECON 212°                 </div> - <div style="border: 1px solid black; padding: 5px; display: inline-block;">                     4 NO DECON INSTRUMENT DEPH 93°                 </div> = 119°	RECORDING SYSTEM 112°	7°	
<div style="border: 1px solid black; padding: 5px; display: inline-block;">                     2 PRE/FILTER + SPIKING DECON 125°                 </div> - <div style="border: 1px solid black; padding: 5px; display: inline-block;">                     3 NO DECON 212°                 </div> = -87°	PROCESSING (SECTION 2) -95°	8°	

Fig. 28. Phase differences calculated from wavelet-extraction results.

## CONCLUSIONS

It has been demonstrated that an estimate of the seismic wavelet can be made by correlating seismic data with well-log data. A method has been outlined that attempts to converge to a stable wavelet solution in spite of small errors in the log and seismic data. The method depends on finding optimum windows for the extraction process, and results in an average wavelet for some time and space interval around the well-log location.

Two real data cases were presented. The first case showed that the average linear phase values calculated from four wells in a given area differed by no more than 22 degrees, and that the extracted wavelets were visually very similar. The second case showed that the wavelet-extraction procedure could be used to evaluate the results of various processing sequences, and correct the phase errors introduced by each sequence.

## REFERENCES

- Berkhout, A.J., 1974, Related properties of minimum-phase and zero-phase time functions: *Geophysical Prospecting*, v. 22, p. 683-709.
- , 1977, Least-squares inverse filtering and wavelet deconvolution: *Geophysics*, v. 42, p. 1369-1383.
- Neale, G.H., 1977, Effects of field recording filters on the seismic wavelet: Presented at the Forty-seventh Annual Meeting of the SEG, Calgary.
- Thomas, D.H., 1977, Seismic applications of sonic logs: Presented at the Fifth European SPWLA Logging Symposium, Paris, France.
- Thompson, D.D., 1979, Phase bias in seismic processing: Presented at the Forty-ninth Annual Meeting of the SEG, New Orleans.
- White, R.E., 1980, Partial coherence matching of synthetic seismograms with seismic traces: *Geophysical Prospecting*, v. 28, p. 333-358.

## APPENDIX

Wavelets observed in practice (instrument responses, source signatures, etc.) often have phase spectra that are essentially linear over a limited bandwidth. A linear phase spectrum will produce two effects during convolution: a time-shift, measured by the slope of the phase spectrum, and a constant phase rotation, measured by the intercept with the phase axis. By analogy, the time zero of any wavelet can be defined as the average time shift, measured by the slope of a line fitted through the phase spectrum by the least-squares method.

The calculation of time zero is made in the following way. The phase spectrum  $P(f)$  and the amplitude spectrum  $A(f)$  are computed. If the wavelet is denoted by  $w(t)$  and its Fourier Transform by  $W(f)$  then

$$W(f) = A(f) \exp(-j.P(f))$$

where both  $A(f)$  and  $P(f)$  are real functions of frequency  $f$ , and  $j = \sqrt{-1}$ .

A linear regression is performed on the weighted phase spectrum. More precisely, the error function  $E(m,c)$  is minimised, where  $E(m,c)$  is given by

$$E(m,c) = \int_{-1/2}^{1/2} A^2(f) \cdot \left[ P(f) - (mf + c) \right]^2 \cdot df$$

$m$  and  $c$  are the parameters of the least-squared error line. It can easily be shown that

$$m = \frac{\int A^2(f) \cdot f \cdot c \cdot df + \int A^2(f) \cdot f \cdot P(f) \cdot df}{\int A^2(f) \cdot f^2 \cdot df}$$

and since  $A(f)$  is an even function,  $[A(f) = A(-f)]$

$$\int A^2(f) \cdot f \cdot c \cdot df = 0 \quad \int A^2(f) \cdot f^2 \cdot df = K,$$

$$m = 1/K \int A^2(f) \cdot f \cdot P(f) \cdot df$$

From the linear phase shift property of the Fourier Transform, " $m$ " is, in fact, the time shift required.